Journal of Electronic Materials
https://doi.org/10.1007/s11664-023-10633-1

ORIGINAL RESEARCH ARTICLE

Comparative Study of the Synthesis and Characterization of Reduced Graphene Oxide (RGO) Using an Eco-Friendly Reducing Agent

F. M. F. Galvão[1] · R. L. B. Cabral[1] · E. V. Santos[1,2] · J. E. L. Santos[2] · T. F. Santos[1] · A. Zille[3] · A. L. A. Mattos[4] · D. F. S. Souza[1] · J. H. O. Nascimento[1]

Received: 16 March 2023 / Accepted: 20 July 2023

Abstract

In this work, the reducing action of four reducing agents—ascorbic acid, inorganic salt, sodium hydrosulfite and polysaccharide—was investigated. Some reducing agents, in addition to being environmentally friendly, are good substitutes for dangerous chemicals used industrially. Graphene oxide (GO) was synthesized by the modified Hummers method and was reduced with ascorbic acid (RGO-AA), inorganic salt (RGO-SI), sodium hydrosulfite (RGO-HS) and polysaccharide (RGO-PS). The microstructural, morphological, optical, electrochemical and thermal properties of GO, RGO-AA, RGO-SI, RGO-HS and RGO-PS were characterized by x-ray diffraction (XRD), Raman spectroscopy, Fourier transform infrared spectroscopy/attenuated total reflectance (FTIR-ATR), x-ray photoelectron spectroscopy (XPS), high-resolution transmission electron microscopy (HRTEM)/energy-dispersive x-ray spectroscopy (EDS), field-emission scanning electron microscopy (FEG-SEM), UV–Vis, zeta potential, thermogravimetric analysis (TGA) and differential scanning calorimetry (DSC). The conclusive results showed that the four agents demonstrated reducing capability. It was observed that the reducing agent derived from inverted sugar (polysaccharide) was the most efficient because it presented a reduction in GO with fewer microstructural defects, a lower number of sheets, and electrochemical and thermal properties superior to the properties obtained from conventional reducing agents. Therefore, with these impressive results obtained with polysaccharide, it was concluded that an effective GO reducing agent was obtained using this green and ecological product, resulting in a reduced graphene oxide (RGO) with few sheets and fewer defects and, consequently, with greater supercapacitor application potential.

Keywords Graphene oxide · agent reducers · polysaccharide · electrochemistry properties · supercapacitors

Introduction

After the innovative demonstration of the electric field effect of graphene reported more than a decade ago and subsequent exploration of its superior physical, chemical and mechanical properties, this 2D nanomaterial has been the subject of numerous studies and applications. The unique properties of graphene have driven the exploration of its potential application in technologies of the new industrial revolution[1] such as high-speed transistors,[2] flexible displays for smartphones and TVs,[3] solar cells,[4] supercapacitive batteries,[5] smart cars, and[6] wearable technologies (fibertronics),[7] among others.[1] This has motivated the drive for the commercialization and availability of graphene in the form of flakes, produced on the order of a few tens of tons and meters in length per year, in the form of continuous sheets, with an estimated value of US$ 100 million by 2021.[8]

✉ F. M. F. Galvão
felipefmfg@gmail.com

✉ J. H. O. Nascimento
heriberto.nascimento@ufrn.br

1 Postgraduate Program in Chemical Engineering, Center of Technology, Federal University of Rio Grande do Norte, Natal, Rio Grande do Norte 59072-970, Brazil

2 Environmental and Applied Electrochemical Laboratory, School of Science and Technology, Federal University of Rio Grande do Norte, Lagoa Nova, Natal CEP 59078-970, Brazil

3 Center for Textile Science and Technology (2C2T), University of Minho, 4800058 Guimarães, Portugal

4 Embrapa Agroindústria Tropical, Planalto do Pici, Fortaleza, CE, Brazil

Published online: 21 August 2023

Pure graphene is obtained mainly through chemical vapor deposition (CVD) in high-vacuum conditions at temperatures up to 1000°C, using gases such as methane as a carbon source or by graphitization of the surface of single crystals of silicon carbide.[8,9] Therefore, these methods are time-consuming and costly, and still present technological difficulties for the industrial-scale production of graphene-based devices. As a result, many studies have been undertaken to explore various alternative approaches for the low-cost and large-scale production of graphene.[10]

For this purpose, the synthesis of graphite oxide (GO) has been explored as an alternative to obtain graphene products on an industrial and economical scale, using classic graphite chemical exfoliation methods[11,12] such as those used by Brodie, who oxidized graphite for the first time over 150 years ago with a mixture of $KClO_3$ and nitric acid,[13] or another century-old method, proposed by Staudenmaier, who oxidized graphite with HNO_3/H_2SO_4 in a 1:2 ratio in the presence of $KClO_3$.[14] Later methods included those of Hummers, Hoffman and Offeman,[11] who used a mixture of sulfuric acid, sodium nitrate and potassium permanganate. This method is considered efficient and is widely used to prepare GO nanosheets.[15,16] Other methods include electrochemical,[17] microwave-assisted[18] and solvothermal techniques,[19] which offer fast and efficient processes for exfoliation of graphite.

Thus, GO is known to be a sheet of graphene with various oxygenated functional groups (OFGs) covalently bonded on its surface, which are responsible for the hydrophilicity of the material. However, the biggest disadvantage of GO, mainly as a material for modifying the surfaces of electrodes, capacitors and flexible batteries, is its high electrical resistance.[20] While graphene only has conjugated sp^2 hybridized carbons in its structure, GO has a full surface composed of covalently bonded OFGs and defects in its structure, which can interrupt the conjugation, giving rise to domains with sp^3 carbons and decreasing the electrical conductivity of GO in relation to graphene.[21]

In order to overcome this problem, the reduction of GO to RGO is typically carried out in order to remove the oxygenated groups, restoring the graphene properties. For example, GO exhibits sheet strength greater than 1×104 S cm^{-1} while values on the order of 1×103 S cm^{-1} and 400 S cm^{-1} are found for RGO and pure graphene, respectively. In contrast to GO, RGO can have its sp^2 conjugated carbon structure largely restored depending on the experimental conditions applied to carry out the reduction, thus increasing its electronic conductivity, as well as a color change from brown to black, increased hydrophobicity and C/O ratio, and consequent aggregation of sheets and the elimination of OFGs from the surface of RGO sheets.[21–23] Although several studies have been dedicated to the development of GO reduction methods, further studies are still needed to achieve appropriate improvements for the development of new reduction methods. As a result of the intense oxidation during the chemical exfoliation of the graphite, residual OFGs and defects remain in the sheet, resulting in structural and electronic differences.[23]

Therefore, several reduction methods have been studied, including the application of laser[24] and chemical reduction using aggressive chemical reducing agents such as hydrazine,[25] ammonia[26] and the most commonly studied, sodium borohydride[27] and sodium hydrosulfite.[28] These are considered dangerous reducing agents, which makes their use impractical in industrial application. Various other reducing agents have been investigated, including ascorbic acid,[29] amino acids,[30] sugars,[31] spices such as cinnamon,[32] plant extracts,[33–36] and fruits such as jambo[37] and white currant.[38] In this research work, new reducing agents were evaluated to obtain RGO, one eco-friendly and the other stable but non-eco-friendly, both used in the reduction of polyester fibers in the textile industry. They were then compared with previously studied reducing agents such as ascorbic acid (eco-friendly) and sodium hydrosulfite (non-eco-friendly), and it was determined which parameters were influenced by the respective reducers in obtaining the RGO.

Materials and Methods

The chemicals used in the GO synthesis process included graphite powder (Vonder®), sodium nitrate (Dinâmica®), sulfuric acid P.A. (H_2SO_4), potassium permanganate ($KMnO_4$), hydrogen peroxide (H_2O_2), and hydrochloric acid (HCl), all from LabSynth® Products Laboratories). All products were used as received without further purification. GO was synthesized using the modified method of Hummers and Hoffman, followed by sonication.

Synthesis of GO

In a beaker, 1 g of graphite powder and 0.5 g of sodium nitrate were added, followed by the addition of 23 mL of sulfuric acid P.A., under constant stirring at 500 rpm for 1 h. Then, 3 g of $KMnO_4$ was gradually added to the above solution, keeping the temperature below 20°C to avoid overheating. The resulting mixture was stirred for 12 h with the temperature controlled at 35°C, and the resulting solution was diluted by adding 500 mL of water under vigorous stirring. To ensure completion of the reaction, the solution was treated with 5 mL of hydrogen peroxide (H_2O_2). Finally, the mixture was washed with hydrochloric acid (HCl) followed by distilled H_2O. To obtain the GO, the solution was sonicated in an ultrasonic bath for 2 h, using a Sacch® UC40/3PT ultrasound instrument, as shown in the schematic of Fig. 1a.

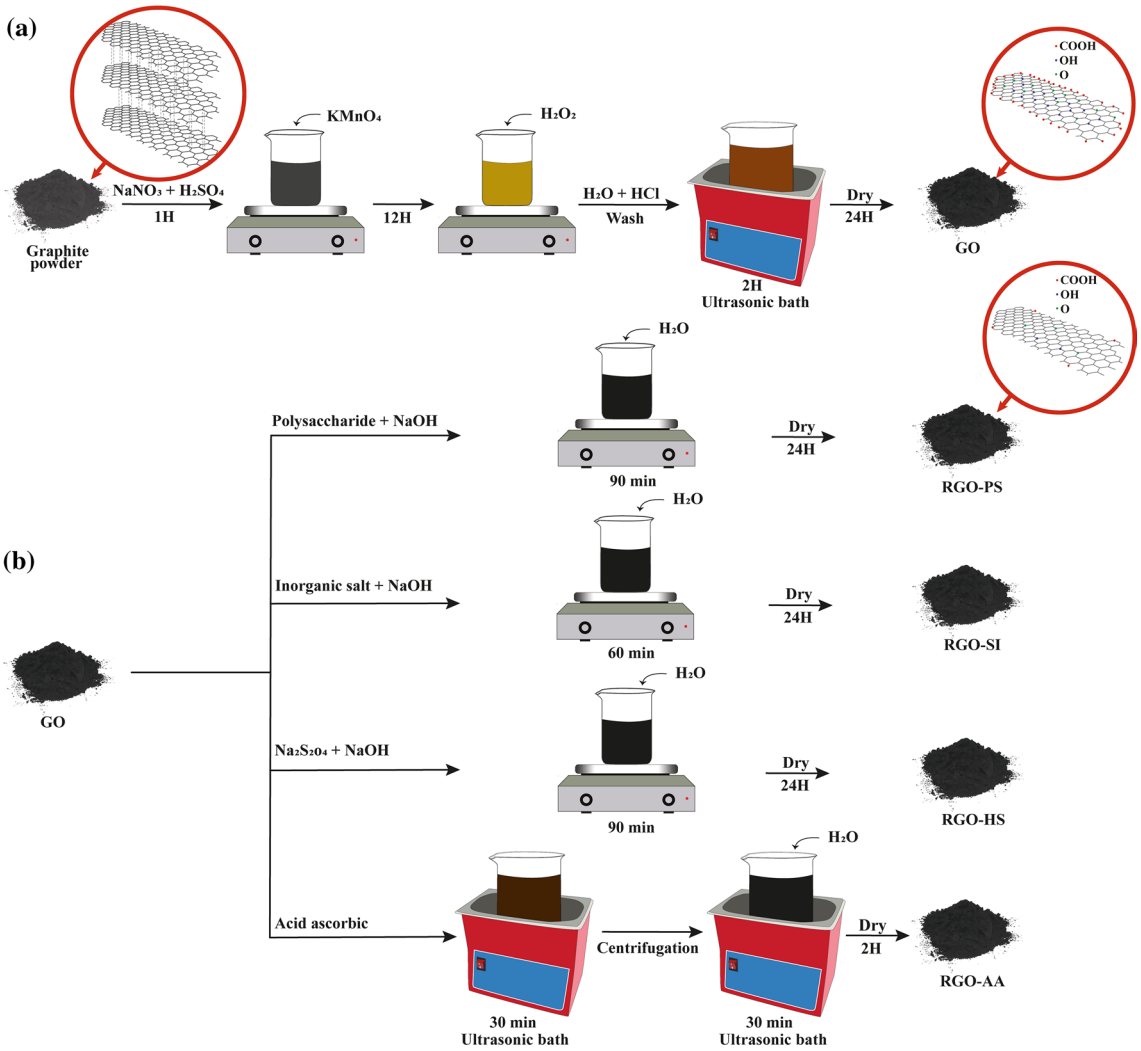

Fig. 1 Flowchart of the process used to obtain reduced graphene oxide with different reducing agents.

Synthesis of RGO

For the different GO reduction processes, the following were used: ascorbic acid (AA) and H_2O_2 (LabSynth®), and sodium hydrosulfite (HS) and sodium hydroxide (Dinâmica®), which were used to adjust the pH of the bath and enhance the dispersion of the GO. Additionally, inorganic salt (SI) and polysaccharide (PS) were provided by Golden Technology. The reducing agents are exhibited in Table I and shown in the schematic of Fig. 1b.

Reduction with PS

PS, a non-volatile and non-flammable liquid, is an industrial and ecologically friendly reducing agent. Its composition is basically based on inverted sugar, that is, the decomposition of sucrose into glucose and fructose after hydrolysis. Therefore, it is considered an ecologically friendly product, and is mainly used in the textile industry to reduce polyester fibers and their mixtures with cellulosic fibers for better efficiency in the dyeing process.

Table I Description of samples

Sample	Description	Reducing agent
RGO-AA	Reduced graphene oxide (RGO)	Ascorbic acid
RGO-SI		Inorganic salt
RGO-PS		Polysaccharide
RGO-HS		Sodium hydrosulfite

Given its characteristics and advantages as an ecologically friendly reducing agent, it was used as a practical and ecologically sound alternative to reduce GO and transform it into RGO. For this process, 0.3 g of GO in 150 mL of distilled water was used plus 4.0 g/L of PS (Golden Technology) and 2.0 g/L of NaOH (sodium hydroxide) (Dinâmica®)

at 90°C for 90 min under vigorous stirring on a heated plate equipped with a magnetic stirrer. After this period, the color of the solution changed from brown to black, indicating the reduction of GO with the PS. The RGO obtained was washed three times for 30 min with distilled water and filtered. The RGO was then dried in an oven at 60°C for 24 h and designated as RGO-PS.

Reduction with SI

SI is an industrial reducing agent, a non-flammable powder, used for reductive washes after dyeing polyester and mixtures with cellulosic fibers. Given its applicability, this product has emerged as an alternative to carry out reduction of GO into RGO. To obtain the RGO, 0.3 g of GO was placed in 150 mL of distilled water plus 4.0 g/L of SI (Golden Technology) and 2.0 g/L of sodium hydroxide (NaOH) (Dinâmica®) at 90°C for 1 h under vigorous stirring on a heated plate equipped with a magnetic stirrer. After this period, the color of the solution changed from brown to black, indicating the reduction of GO with the SI. The RGO obtained was washed three times for 30 min with distilled water and filtered to remove residual N_2H_4 from the solution. The RGO was then dried in an oven at 60°C for 24 h and designated as RGO-SI.

Reduction with HS

In this case, 0.5 g of GO was dispersed in 250 mL of distilled water. Then, 1.25 g of sodium hydrosulfite (Dinâmica®) and 1.0 g of sodium hydroxide (Dinâmica®) were added to the solution. The solution was stirred and maintained at 90°C on a heated plate equipped with a magnetic stirrer for 90 min. After this period, the color of the solution changed from dark brown to black, indicating that GO was reduced by HS. The obtained RGO was washed three times with distilled water, followed by filtration. The black filtrate was then oven-dried at 60°C for 24 h and designated as RGO-HS.

Reduction with AA

To reduce GO, 0.3 g of GO and 0.2 mol/L of AA (vitamin C, Synth®) were used. In this mixture, 150 mL of distilled water was added and the solution was sonicated for 30 min at 60°C. The reduction products were centrifuged at 600 rpm to remove the supernatant. Then, 30% H_2O_2 (LabSynth®) was added to the suspension to oxidize the remaining AA and then sonicated for 30 min at 60°C. Because of the low rate of reduction, AA needs the addition of H_2O_2 to facilitate its reduction, in addition to enhancing the cleaning of GO after reduction. After sonication, the resulting mixture was centrifuged at 600 rpm, washed three times with ethanol and distilled water, respectively, and dried at 120°C for 2 h. The reduced graphene was designated as RGO-AA.

Characterization

The structural characterization of GO and RGO was conducted by x-ray diffraction (XRD). A Rigaku MiniFlex II universal x-ray diffractometer was used, with a copper (Cu) radiation source, power of 30 kV and current of 30 mA, in the angular region of 10°–90° with step 0.02 and speed of 5°/min. Raman spectroscopy was used to identify differences between the D, G and 2D bands in the structures. The Raman analyses were carried out on a Horiba LabRAM Evolution spectrometer using a laser with a wavelength of 532 nm, intensity of 1%, optical zoom of 50×, with 10 s of irradiation with 10 accumulations and scanning range from 198 cm^{-1} to 3326 cm^{-1}. The Fourier transform infrared (FTIR) spectra of the samples were recorded using a Shimadzu IRTracer-100 spectrometer with a resolution of 4 cm^{-1} and a spectral range of 4000 cm^{-1} to 400 cm^{-1}. Chemical analysis of the GO and RGO samples was performed by x-ray photoelectron spectroscopy (XPS) using a VG Scientific instrument, with ESCALAB 200A data acquisition software (UK). The spectrometer was calibrated with reference to the Ag 3*d*5/2 line (368.27 eV) and was operated in CAE mode with a pass energy of 20 eV. This analysis was carried out in an ultra-vacuum environment ($\sim 1.3 \times 10^{-9}$ KPa) using achromatic Kα radiation from an Al anode operating at 15 kV (300 W) as an excitation source. The obtained spectrum was modulated through XPSPEAK software, using the position of the C 1*s* carbon line as reference, at 285 eV. Data analysis was performed using peak fitting with a Gaussian–Lorentzian form and Shirley background subtraction (or linear, depending on the data) and least squares routine for adjusting the position of the spectral lines. High-resolution transmission electron microscopy (HRTEM) and selected area electron diffraction (SAED) images were obtained with a JEOL JEM-2100 microscope operating at 200 kV and with a resolution of 0.2 nm used to show the structural properties of GO and RGO samples. The specific surface areas of the GO and all RGO were calculated by the Brunauer–Emmett–Teller (BET) method from the adsorption isotherms on a Quantachrome Nova 2200E surface analyzer. The samples were analyzed under a nitrogen atmosphere (adsorption-desorption isotherms at 77 K) in a volumetric working device. A drop of the solution was deposited on a copper grid covered with a carbon film and placed in the sample holder. Field emission scanning electron microscopy (FEG-SEM) was carried out on a Carl Zeiss Supra 35-VP microscope, where the samples were treated with gold deposited in vacuum for 3 min. Zeta potential analysis was performed using a Malvern

Zetasizer Nano ZS. For this analysis, the solutions of GO and RGO samples were prepared using a concentration of 0.005 g/mL^{-1} in Milli-Q water. The pH of the samples was previously altered using acetic acid and sodium hydroxide, both with a concentration of 5%, varying from pH 2 to pH 14. UV–Vis spectroscopy of GO and RGO were obtained using a Shimadzu UV-2600 spectrophotometer operating in absorbance mode, equipped with an ISR 240A integration sphere and UVPC software. Scans were performed between 200 nm and 400 nm.

Thermal Characterization

Thermogravimetric Analysis (TGA) and Differential Scanning Calorimetry (DSC)

The thermal characterization of GO and RGO was carried out via TGA/DSC in a nitrogen atmosphere and a temperature range between 25°C and 1000°C with a heating rate of 10°C min^{-1} and a nitrogen flow rate of 150 mL/min, using a Shimadzu TGA-51/51H analyzer. It was also evaluated via DSC over a temperature range from 25°C to 400°C at a rate of 10°C min^{-1} in a nitrogen atmosphere with a flow rate of 20 mL min^{-1} using a PerkinElmer instrument.

Electrochemical Analysis

To investigate the electrical properties of the GO and RGO samples, electrochemical analysis was carried out using cyclic voltammetry (CV) and impedance spectroscopy. For this, a modified electrode consisting of a virgin copper-plated phenolite plate as metallic contact was developed (Fig. 2a). The phenolite plate was cut to dimensions of 2 cm in height by 5 cm in width, and a slit of approximately 1 mm in width was opened to separate the contacts from the copper plate (Fig. 2b). A paste composed of the materials under study was deposited to close the contact, as shown in Fig. 2c. Then, a simple modified electrode was built for reading the CV and impedance of GO and RGO. In this way, more accurate results of their electrical properties could be obtained.

The electrochemical analyses were carried out on a Metrohm Autolab PGSTAT302N potentiostat/galvanostat, coupled to a computer and controlled by Metrohm NOVA 1.8 software for data acquisition and for plotting of the cyclic voltammetry (CV) graphs, galvanostatic curves (GC), and electrical impedance in the potential range of −0.25 V to 1.25 V, with sweep rates of 20 mV/s, 30 mV/s, 40 mV/s, 50 mV/s, 100 mV/s, and 200 mV/s, impedance and galvanostatic charge and discharge curves (CCG) for three cycles, and frequency of 100 kHz to 10 MHz and amplitude of 5 mV.

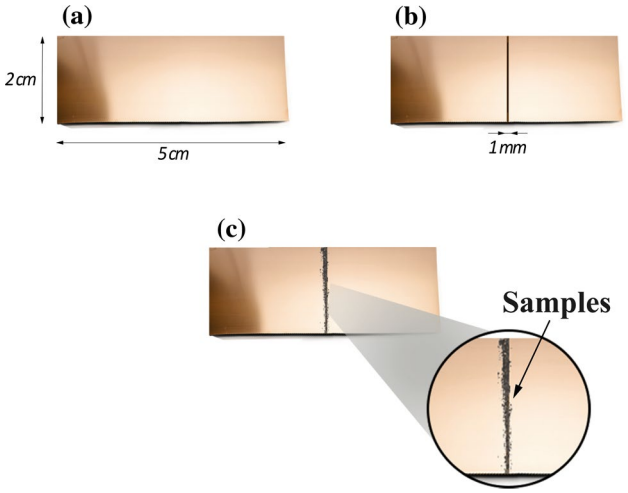

Fig. 2 Illustrative scheme of electrochemical analysis. (a) Phenolite board; (b) demonstration of the cut performed on the plate; (c) deposition of GO and RGO to carry out the electrochemical test.

Results and Discussion

Microstructural Characterization

X-Ray Diffraction

The process of synthesis was carried out to obtain GO from graphite using the method of Hummers and Hoffman with additional sonication. The diffractogram in Fig. 3a was obtained over a scanning range from 0° to 70°. The appearance of a peak intensity was observed at $2\theta = 11.8°$, which is attributed to the interplanar spacing in the d_{002} direction, caused by the intercalation of hydroxyl, epoxy and carboxyl functional groups between the GO sheets in particular in the basal planes on both sides of the GO sheets.

The position of the GO peak mainly depends on the degree of graphite oxidation: the greater the spacing between layers for GO, the greater the order of oxidation and exfoliation. There are also peaks of lesser intensity highlighted in the region $2\theta = 26°$ related to the presence of graphite impurities.[39] After the reduction of GO with different reducers, different behaviors of the diffraction peak (002) were verified; however, in all reductions there was a restoration of the ordered crystalline structure of RGO and removal of most oxygen functional groups, as exhibited in Fig. 3. This is verified by the reappearance of the diffraction peak (002) at $2\theta = 22.4°$ for RGO-AA (Fig. 3b), $2\theta = 26.1°$ for RGO-HS (Fig. 3c), $2\theta = 25.8°$ for RGO-SI (Fig. 3d), and $2\theta = 22.3°$ for RGO-PS (Fig. 3e). The RGO-PS after reduction showed an increased peak and reduced intensity, which indicates that graphene was exfoliated into single-layer or few-layer sheets, and a new network structure significantly different from graphite was formed, with interplanar distance of 4.57 Å,

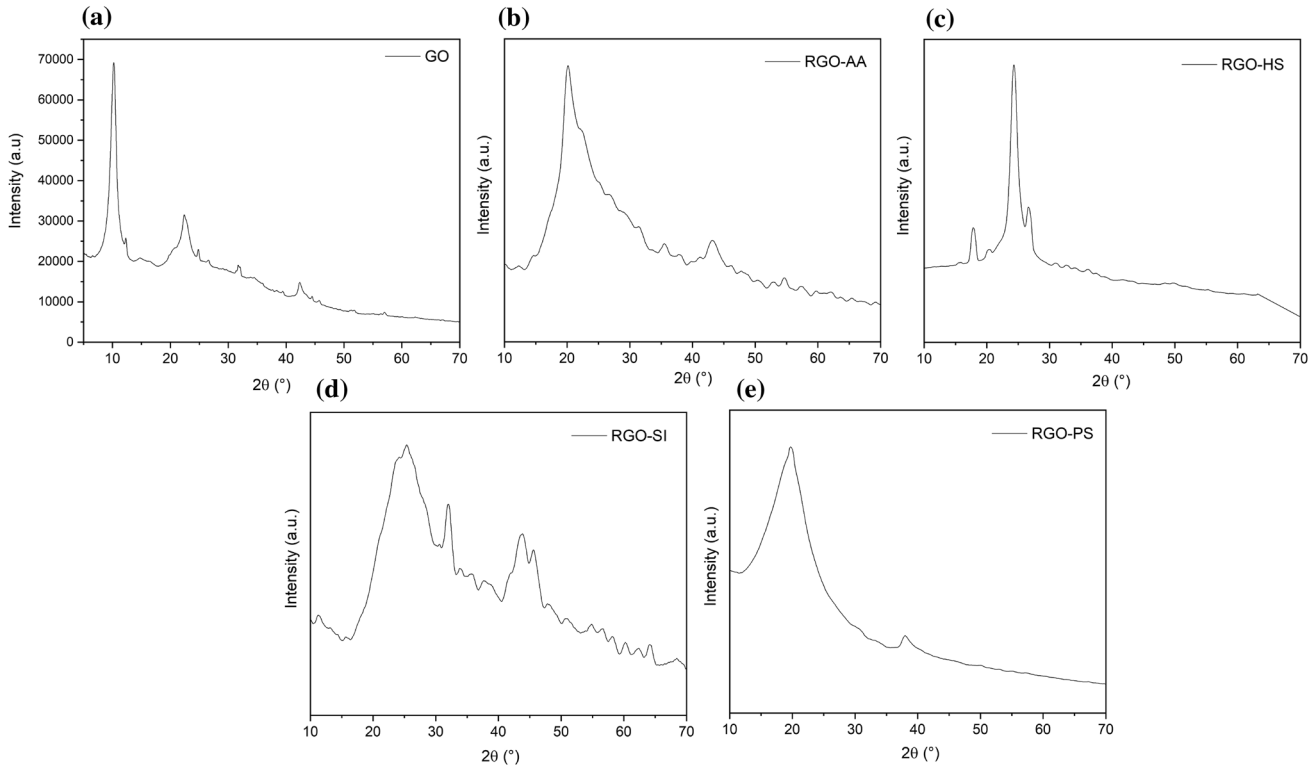

Fig. 3 XRD of synthesized reduced graphene oxide with (a) GO, (b) RGO-AA, (c) RGO-HS, (d) RGO-SI, (e) RGO-PS.

crystallite size of approximately 1 nm and four sheets. RGO-AA showed an interplanar distance of 3.35 Å, crystallite size of approximately 0.66 nm and five sheets. The average crystallite size (D) of GO and RGO was also determined by the Scherrer equation (Eq. 1), as follows:

$$D = \frac{k\lambda}{\beta \cos\theta} \tag{1}$$

where λ is the wavelength of the incident x-ray beam (1.54 Å for Cu-Kα), θ is the Bragg diffraction angle, β is the full width at half maximum of the peak of greatest intensity in radians, and 0.90 is the constant for spherical crystallites.

The RGO-SI, in turn, presented an interplanar distance of 3.65 Å and a crystallite size of approximately 3.33 nm, and the RGO-HS presented an interplanar distance of 4.08 Å and crystallite size of approximately 0.88 nm, and comprised four sheets.[28,40] That is, RGO-PS has the same number of sheets as the RGO-HS, which demonstrates the efficiency of the reducer with eco-friendly properties.

Raman Spectroscopy

The Raman spectra obtained for GO are shown in Fig. 4a. In the syntheses of RGO with different reducers as shown in Fig. 4b, it was observed that both RGO-AA and RGO-HS have G-band peaks at 1580 cm^{-1}, which are more intense than the D-band peaks at 1351 cm^{-1}, although RGO-HS exhibited peaks with greater intensity. Unlike previous syntheses, RGO-SI and RGO-PS have D-band peaks at 1351 cm^{-1}, which are more intense than the G-band peaks at 1580 cm^{-1}. Furthermore, the ratio of the D- and G-band (I_D/I_G) intensity is an estimate of the degree of disorder in the graphitic structure of these materials. It is inversely proportional to the average size of the sp^2 clusters, and the higher the ratio of RGO to GO, the better the efficiency and accumulation in the sp^2 surface area.[29,41] The ratios for materials synthesized with different reducers were obtained as 0.97 for RGO-AA, 0.97 for RGO-HS, 1.01 for RGO-SI and 1.05 for RGO-PS.

Fourier Transform Infrared Spectroscopy and Attenuated Total Reflectance (FTIR-ATR)

FTIR spectroscopy was used to determine the functional groups present in (GO) and RGO with different reducing agents. The analyzed spectra comprised scanning in a wavelength region between 4000 cm^{-1} to 500 cm^{-1}. The spectrum of GO, shown in Fig. 5, demonstrates the presence of several oxygen-containing functional groups attached to the graphite network. Elongation vibrations of the C–O epoxy group were observed for the band at 1043 cm^{-1}, and

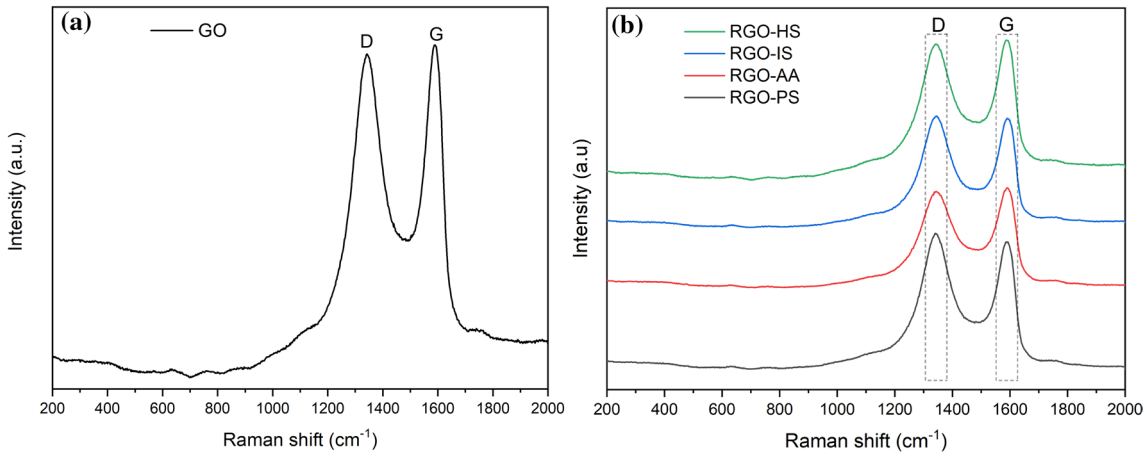

Fig. 4 Raman spectra of (a) GO and (b) RGO synthesized using different reducing agents.

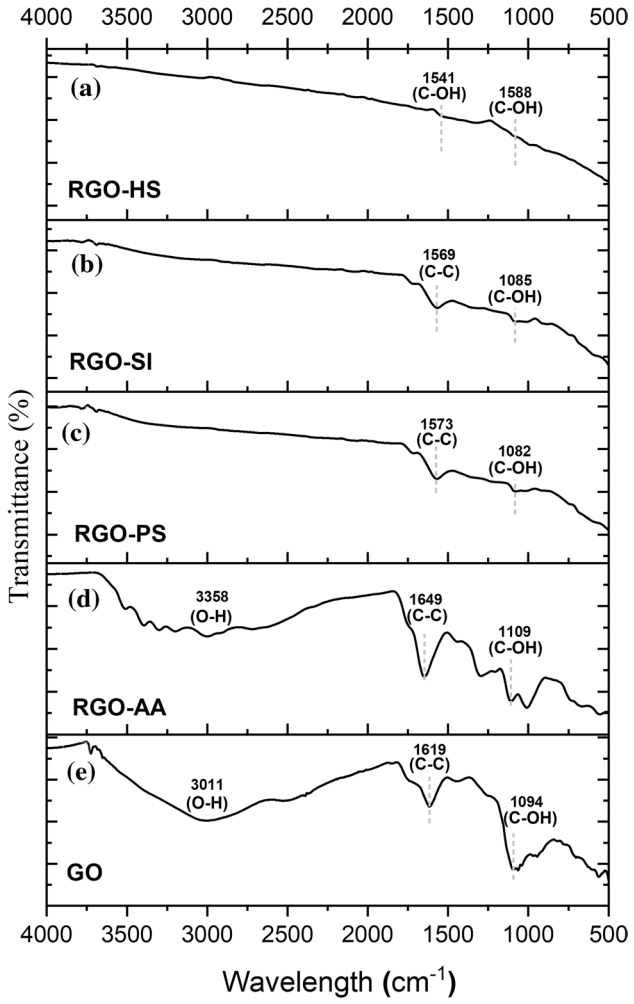

Fig. 5 FTIR spectra of RGO with different reducing agents: (a) RGO-HS, (b) RGO-SI, (c) RGO-PS, (d) RGO-AA. FTIR spectrum of (e) GO.

its wider opening reveals the presence of alcohols and phenols. The peaks at 3011 cm^{-1} and 1619 cm^{-1} were attributed to the stretching and deformation vibrations of the hydroxyl groups, respectively. Furthermore, the peak at 1619 cm^{-1} exhibits C–C groups, while a small band at 1580 cm^{-1} was attributed to aromatic carbon.[42,43]

According to the FTIR results obtained in the reduced samples, a significant change in the spectra of the RGO samples was observed. The peaks corresponding to the functional groups containing oxygen such as hydroxyls and alkoxy were suppressed, mainly in the sample with the reduction carried out with polysaccharide (RGO-PS), as shown in Fig. 5c, which confirms that the reduction of GO using this reducing agent was identical to the reduction using SI and HS, and with the advantage of being ecologically viable.[44] Shifts in the spectrum of RGO-PS show the appearance of new peaks of lesser intensity in the region corresponding to the bands at 1082 cm^{-1} and 1573 cm^{-1} for C–OH and C–C groups, respectively.[45] The spectral characteristics are similar for RGO-SI, showing peaks in this case at 1085 cm^{-1} and 1566 cm^{-1} as shown in Fig. 5b.[44,45] In the reduction of RGO-HS, the peaks were considerably weakened, as exhibited in Fig. 5a, which may be related to a low reduction temperature.[46] For the reduction of GO using AA (RGO-AA), although presenting peaks of lesser intensity in the region of 1109 cm^{-1} corresponding to the C–OH group and to the C–C group at a wavelength of 1649 cm^{-1}, it still showed a marked widening in the region at 2500–3500 cm^{-1}, attributed to the oxygenated groups characteristic of GO (Fig. 5e), thus demonstrating inefficient reduction using AA, as shown in Fig. 5d.[44]

X-Ray Photoelectron Spectroscopy (XPS)

The synthesized samples of GO and RGO-PS were analyzed by XPS to complement the results obtained in the

identification of functional groups. The scanning spectra of the respective samples prove the presence of C 1*s* and O 1*s*, according to XPS spectra exhibited in Fig. 6a.

For the GO sample, C 1*s* presents a range of peaks between 280.3 eV and 292.1 eV, which corresponds to 71.16% of the spectral region. For O 1*s*, the peak range is between 527.1 eV and 539.7 eV, which corresponds to 28.84%. The high-resolution spectrum of the peak level of C 1*s* shows four spectral components that correspond to different functional groups of carbon, as shown in Fig. 6a. The non-oxygenated C=C (sp^2) present in the aromatic ring of GO appears at 284.7 eV and the C in the C–OH or epoxy bonds at 285.8 eV. The C(C=O) carbonyl/quinone group was identified at 287.28 eV, and the carboxylate group OH–C=O at 289.8 eV. Thus, the peak level of the core O 1*s* consists of three functional components of O, one at 531.8 eV, corresponding to C=O, C–OH at 532.9 eV and C–O–C at 533.3 eV (Fig. 6b). These results of the C 1*s* and O 1*s* peaks are confirmed in the model proposed by Lerf–Klinowski, where the GO spectra consisted mainly of hydroxyl and epoxy functional groups and, to a lesser extent, quinone/carbonyl and carboxyl.[45,47,48] As for the RGO-PS sample, the C 1*s* peak also presents a range of peaks between 280.3 eV and 292.1 eV, but with a significant increase to 82.18% of the spectrum region. For O 1*s*, there was a decrease to 17.82% in the peak range between 527.1 eV and 539.7 eV. This significant increase confirms the results obtained in the FTIR, where a decrease in oxidized functional groups was verified after reducing treatment with PS. Thus, the functional groups present in the high-resolution spectrum of the peak level of C 1*s* (Fig. 6c) are also the same four spectral components that correspond to different functional groups of carbon, the non-oxygenated C=C (sp^2) present in a larger area and appears in 284.9 eV, the C in the C–OH bonds or epoxy in 286.1 eV. The C(C=O) carbonyl or quinone group was identified at 287.4 eV, and the carboxylic group -COOH at 289.5 eV. Thus, the core peak level O 1*s* also consisted of three functional components of O, one at 531.4 eV, corresponding to OC=O, the C=O corresponding to carbonyl or ketone, at 532.35 eV and at 533.1 eV, C–O–C/C–OH.[49–51]

Morphological Characterization

High-Resolution Transmission Electron Microscopy and Energy-Dispersive X-Ray Spectroscopy: HRTEM/EDS

The HRTEM images shown in Fig. 7 demonstrate the presence of nanosheets for GO and RGO with different reducing agents. It was observed that the material has a good level of translucency, indicating a high degree of graphite exfoliation. It is also observed that the darker regions are related to layers of stacked sheets of GO, where it also presents amorphous and disordered morphology.[52,53] The SAED pattern of GO nanosheets (inset Fig. 7a) showed only diffraction rings and the diffraction points are unresolved, unequivocally indicating that the GO sheets are amorphous. This result is consistent with XRD analysis. The electron diffraction rings obtained by SAED measurements demonstrate interplanar distance *d* at 1.2 Å and 2.1 Å, suggesting the presence of graphitic regions within GO.[54] After chemical reduction with both HS and PS, the GO nanosheets were reduced to RGO nanosheets and restored to an ordered crystalline structure. This is evidenced by the reappearance of the diffraction peak (002) and disappearance of the diffraction peak characteristic of GO according to the XRD analysis. Figure 7b and c show HRTEM micrographs of RGO-HS and RGO-PS, which exhibit morphology of similar, randomly aggregated thin sheets, with distinct edges, wrinkled surfaces and folding. The images obtained show that RGO-HS and RGO-PS nanosheets consist of a few layers ($n < 5$) stacked on top of each other with fewer wrinkles and folds. The insets in Fig. 7b and c show fringes of graphene network according to SAED patterns. This provides additional information

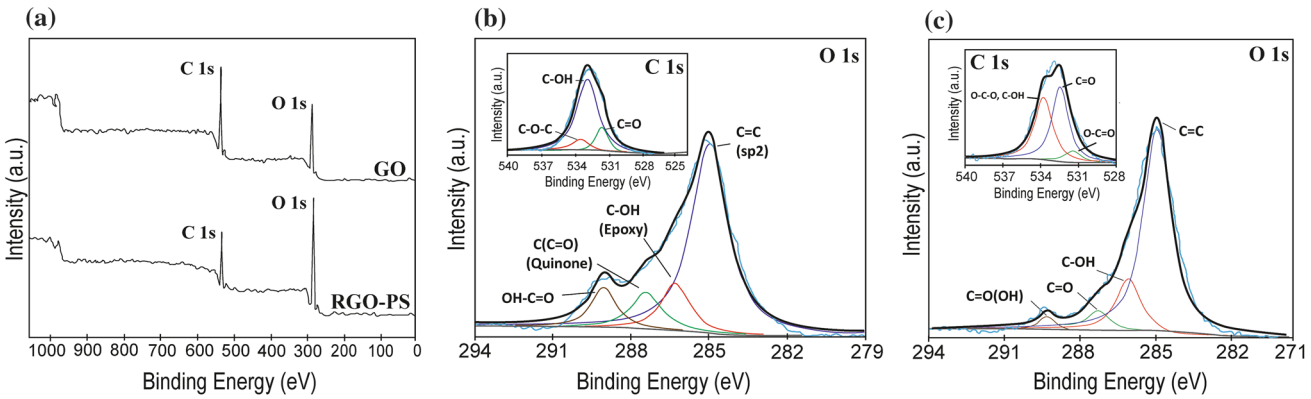

Fig. 6 (a) XPS survey spectra of GO and RGO-PS. High-resolution XPS (C 1*s* and O 1*s*) spectra with deconvoluted peaks of (b) GO and (c) RGO-PS.

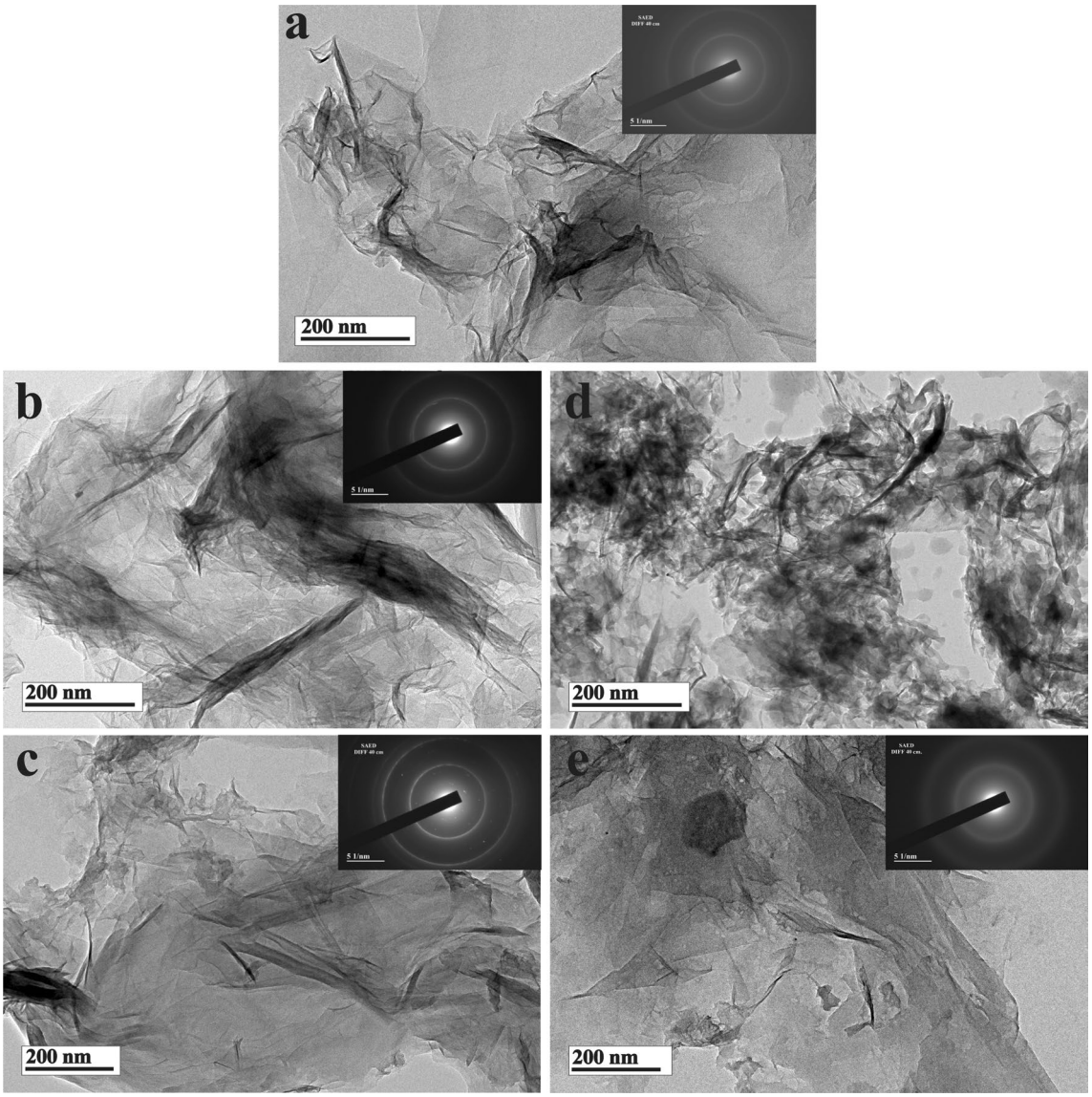

Fig. 7 HRTEM and SAED patterns of (a) GO, (b) RGO-HS, (c) RGO-PS, (d) RGO-SI and (e) RGO-AA.

about the interplanar distance d_{002} for RGO material, whose value is 4.57 Å for RGO-HS and 4.08 Å for RGO-PS. The crystallographic structure of graphene sheets was characterized by SAED. Previous studies mentioned that most graphene sheets exhibit a single set of hexagonal diffraction patterns with sharp and clear diffraction points.[55] Shalaby et al. investigated HRTEM images of RGO and compared the interplanar distance d_{002} of the graphite layers and found that the distance was 3400 Å, which corroborates the literature distinguishing the distances presented from the samples of RGO-HS and RGO-PS.[56] This proves the efficiency of RGO-PS as an ecologically friendly reducing agent. In Fig. 7d, a structure in flakes is observed, which confirms the presence of defects in the graphene sheets. This behavior may be the result of a high reduction caused by the product based on SI and may be one of the factors explaining why the diffractogram is different from that of the other three reducing agents. As a result, this structure made it difficult to obtain the SAED pattern for this sample. In Fig. 7e, RGO-AA demonstrates the formation of an extremely thin film, with a wrinkled structure and the presence of dark spots; however, it presents a fragmented film. These points represent defects in the crystal lattice.[57] RGO-AA presented similar characteristics to the other RGO in this study (except the RGO-SI). The well-defined diffraction dots illustrate that the crystalline state of the AA-reduced GO has been restored, although the discontinuity of fringes and amorphous zones indicate that there are defects in the ascorbic acid-reduced GO sheets.

Specific Surface Area Versus Inter-Sheet Distance (*d*-Spacing)

According to the data obtained from interplanar distance, the samples that present greater interplanar distance have a greater surface area and, consequently, greater conductivity. This is confirmed in studies carried out by Mohan et al.[58] The results obtained in this study show an interplanar distance of 4.57 Å for RGO-PS, 4.08 Å for RGO-HS, 3.65 Å for RGO-SI and 3.35 Å for RGO-AA. According to Fig. 8, the specific surface area results were as follows: 206,283 $m^2\ g^{-1}$ for RGO-AA, 231,164 $m^2\ g^{-1}$ for RGO-SI, 388,207 $m^2\ g^{-1}$ for RGO-HS and 430,622 $m^2\ g^{-1}$ for RGO-PS.[58]

High-Resolution Field-Emission Scanning Electron Microscopy (FEG-SEM)

The morphological and structural evaluation obtained by FEG-SEM of the GO sample can be observed in Fig. 9a and b. The formation of aggregates of GO particles is observed, which is a common behavior observed in microstructural analysis obtained by SEM, even when preparing the sample by simple sonication to remove the aggregates and promoting the separation of the nanosheets to present them individually, when necessary. If the sample is placed on the carbon tape, they may re-aggregate.[59] It is possible to observe a microstructure of GO composed of several layers with a wrinkled appearance and the presence of folds. This wrinkled appearance can be explained by the oxidation process to promote the admission of hydroxyl and epoxy functional groups into its structure, altering the hybridization of sp^2 carbons (plane structure) of graphite to sp^3 (tetrahedral structure) of GO. The formation of these functional groups containing oxygen in the basal planes causes several structural defects in GO, and the greater the degree of oxidation, the greater the spaces between the functionalized layers. Also, chemical methods used to obtain GO from graphite have a relatively good yield, but in general, lead to the formation of irregular and defective structures when compared to bottom-up methods, which are based on the formation of graphene from gases with a high carbon concentration, such as CVD (chemical vapor deposition).[60–62]

After the chemical reduction step with the PS, the morphology of RGO is shown in Fig. 9c and d. When comparing with the FEG-SEM images from GO, a smaller number of sheets is observed, which was previously confirmed by XRD, and there is a greater aggregation of these sheets. This behavior is caused by the reduction of functional groups containing oxygen located in the basal plane of the sp^2 carbon that allows these GO sheets when reduced by PS to be held together by means of weak van der Waals forces.[63]

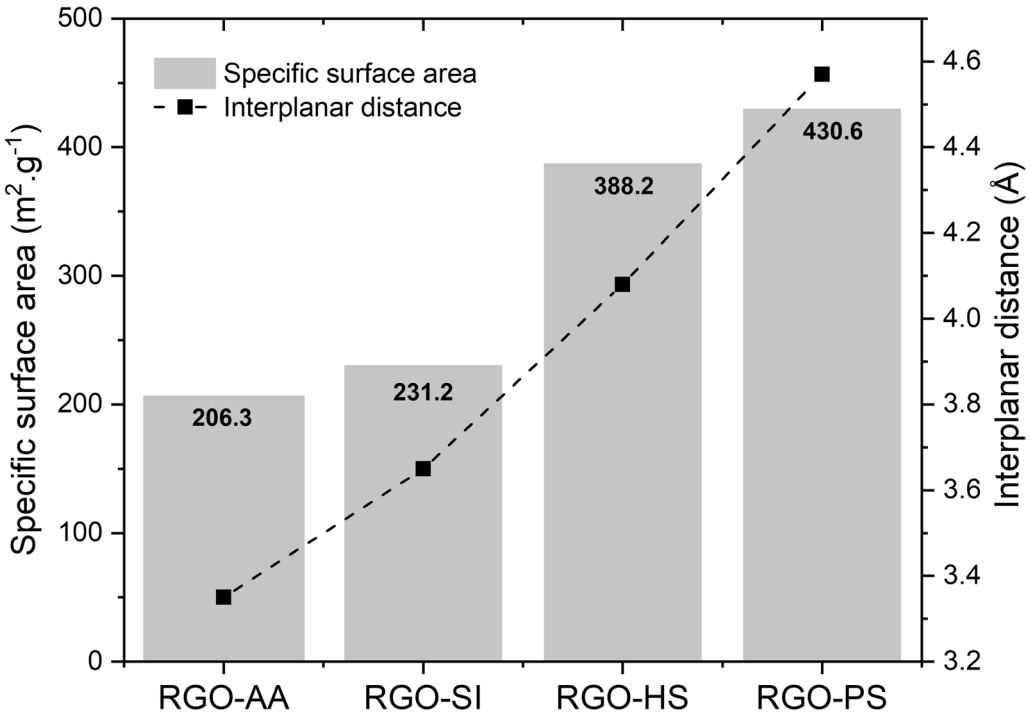

Fig. 8 Comparison plot of specific surface area vs interplanar distance for RGO with different reducing agents.

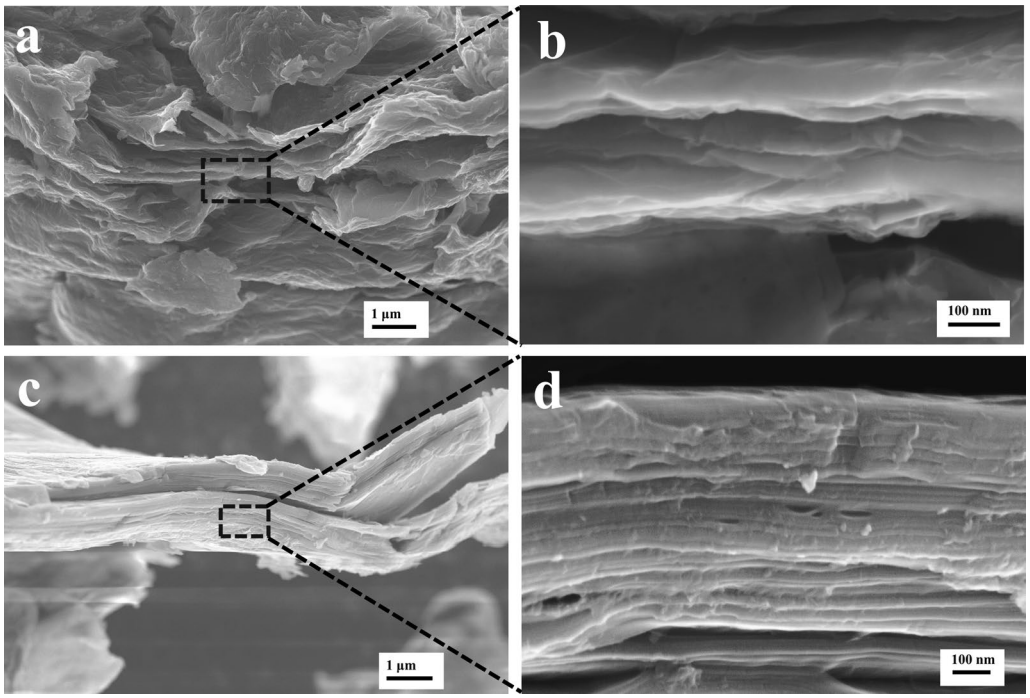

Fig. 9 FEG-SEM images of (a, b) GO and (c, d) RGO-PS at ×10,000 and ×120,000 magnification, respectively.

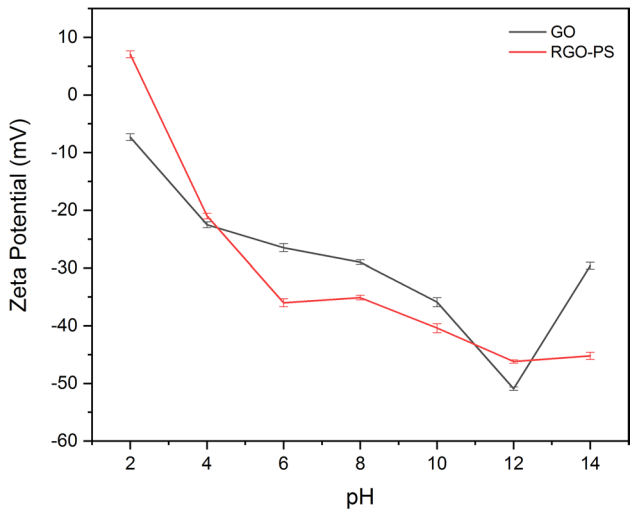

Fig. 10 Zeta potential of GO and RGO-PS at different pH values.

Zeta Potential and UV–Vis Analysis

Zeta Potential

The zeta potential (ζ) was analyzed in different solutions varying the pH values from the most acidic medium (pH = 2) to the most alkaline medium (pH = 14), in order to evaluate the surface charge and stability of GO and RGO, as shown in Fig. 10. As the pH is increased, the surface charge became more negative for GO and RGO. Regarding GO, there was a decrease in charge from −7 mV to −43 mV, which can be explained by the ionization of carboxyl groups present on the surface of GO in response to pH variation. At neutral pH, GO has zeta potential values between −26 mV and 29 mV, which can be attributed to a sufficient mutual repulsive force and formation of stable aqueous dispersion of GO.[64] Regarding the zeta potential of RGO, although at pH of 2 it was positive, from slightly acidic to neutral pH extending to strongly alkaline pH, it showed a lower potential when compared to the result for the GO, with zeta potential of around 35 mV for neutral pH and 45 mV for strongly alkaline pH. This behavior is due to the decrease of the functional groups containing oxygen on the surface, in addition to the loss of negative charge. This significant decrease is attributed to the efficient reduction of GO using PS as reducing agent.[65] This is because particles with zeta potentials more negative than −30 mV generally form stable suspension due to interparticle electrostatic repulsion.[66]

UV–Vis Spectroscopy

UV–Vis spectroscopy is analyzed in the ultraviolet to visible spectrum and was performed to monitor the degree of GO oxidation, shown in Fig. 11a, and RGO with different reducing agents. The absorption peak of the GO dispersion was seen at 248 nm, which corroborates the results of research carried out by Hidayah et al.[67] In UV–Vis spectroscopy, it is

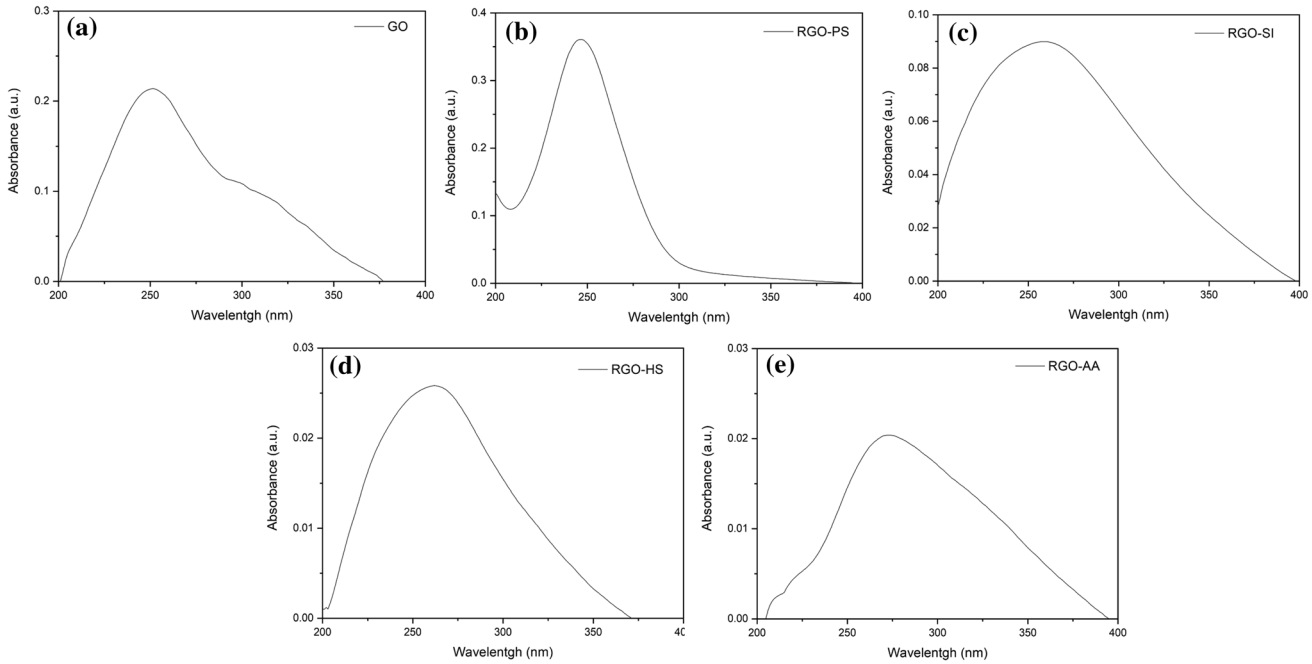

Fig. 11 UV–Vis spectroscopy of (a) GO, (b) RGO-PS, (c) RGO-SI, (d) RGO-AA, (e) RGO-HS.

understood that the optical absorption of GO is named by the *P*–*P** binding peak of the plasmon, which arises due to clusters with sp^2 hybridization of the sheets and their respective binding units. After the GO reduction process (Fig. 11a), there is a shift to the region at 272 nm for RGO-PS, 256 nm for RGO-SI, 250 nm for RGO-HS and 273 nm for RGO-AA, as exhibited in Fig. 11b, c, d, and e. This phenomenon occurs due to the process of desorption of the oxygen bound to the graphene layers and to its π–π^* transition of the graphitic C–C ring. GO nanosheets are hydrophilic, whereas RGO nanosheets are hydrophobic, so it can be seen that while GO is stable in water, RGO has a different behavior, being dispersed homogeneously in water through ultrasonic vibrations, but this dispersion is unstable and shows thermodynamic disequilibrium, with its hydrophobic nature.[68,69]

Thermal Analysis

Thermogravimetric Analysis (TGA) and Differential Scanning Calorimetry (DSC)

Regarding the TGA, it is possible to verify that the loss of mass in GO occurs at temperatures of up to 100°C, shown in Fig. 12a, related to the loss of water molecules absorbed by the structure (approximately 9%) and a slow decomposition of GO. The second stage, which occurs abruptly between 100°C and 250°C (approximately 32%), is related to the elimination of oxygenated hydroxyl, carboxyl and epoxy groups that were inserted in the graphitic structure during oxidation. Further mass losses occur around 250–600°C after the GO reaches its flash point and the solid is decomposed into a carbon residue.[70] This behavior demonstrates a lower thermal stability of GO in relation to RGO-PS, which presented a mass loss of approximately 19%, which is supported by the literature.[71] In Fig. 12b, the DSC analysis shows an endothermic peak around 134°C and enthalpy of 269.7 J/g, which corroborates the TGA analysis, when referring to the loss of water molecules. Another peak, this time exothermic, is presented at 217°C, with enthalpy of 563.9 J/g, in this case indicating the thermal decomposition/exfoliation of GO.[72] For RGO-PS, only a lower intensity endothermic peak is present, related to the loss of water molecules at 137°C and enthalpy of 143.7 J/g.

Electrochemistry

Figure 13a and b show the rectangular traces of the GO and RGO-PS CV curves, respectively. With the sole purpose of confirming that the nanomaterials have electrical properties, only the passage of the current generated by the potentiostat/galvanostat was measured, using the electrode modified with paste of the materials under study. The CV technique measures the current response to a small electrode, obtained as a function of an excitation signal in the form of a triangle. Equation 2 calculates the resistance of the material using Ohm's law:

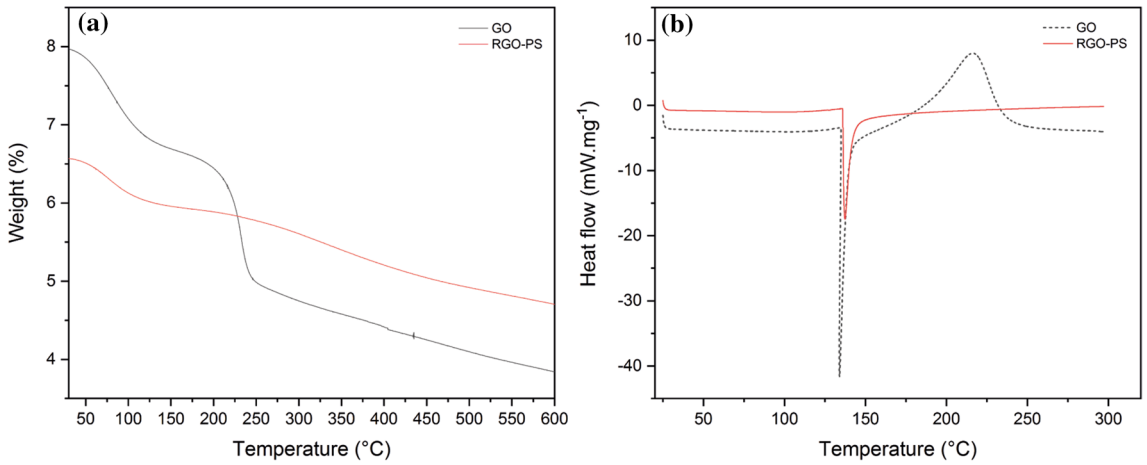

Fig. 12 (a) TGA and (b) DSC analysis of GO and RGO-PS.

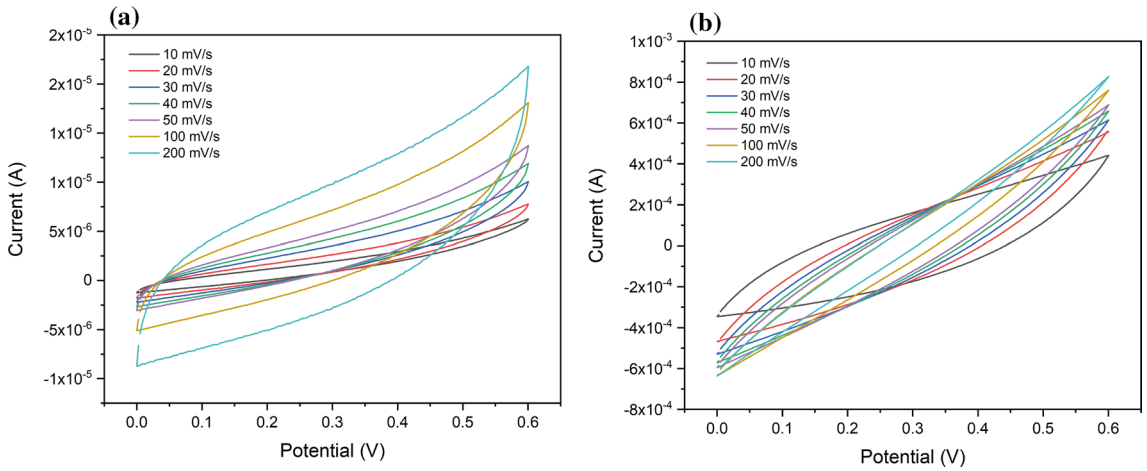

Fig. 13 Cyclic voltammetry of (a) GO and (b) RGO-PS at sweep rates of 10 mV/s, 20 mV/s, 30 mV/s, 40 mV/s, 50 mV/s, 100 mV/s, and 200 mV/s.

$$R = \frac{V}{I} \tag{2}$$

where I is electric current, V is voltage and R is resistance. It is possible to observe a sharp decrease in current for the RGO-PS sample, which implies that this characteristic rectangular shape indicates an ideal electrical double-layer capacitive (EDLC) behavior, according to Zhubin et al.[73] A slight slope also occurs as the scan rate increases, but this slope is considerably reduced in the RGO-PS sample. According to the studies by Choi et al.[74] and Zhu et al.,[75] this is due to the decrease in functional groups, especially oxygenated groups, as evidenced by the XPS analysis. As the velocity rate increases, a significant increase in the electroactive area of RGO-PS is also observed, which can be explained by the surface area and electrical conductivity of the RGO-PS unitary sheets. According to Xu et al.,[76] the formation of a peak with a small increase in the region comprising 0.4–0.6 V may indicate the presence of pseudo-capacitance. According to Couly et al.,[77] the abundant oxygen-containing functional groups in GO can provide this pseudo-capacitance feature, unlike in RGO, where these groups are quenched. Impedance spectroscopy is an effective method to probe the interfacial properties of the analyzed electrodes, in this case GO and RGO-PS.

Figure 14 presents an analysis of the influence of frequency taking into account the phase and real impedance of the material. Impedance spectroscopy allows the determination of capacitance (Cd). It is represented by the letter Z and measured in ohms (Ω). In this method, an alternating current potential with different frequency values is applied. It is possible to measure this value in any electrical circuit

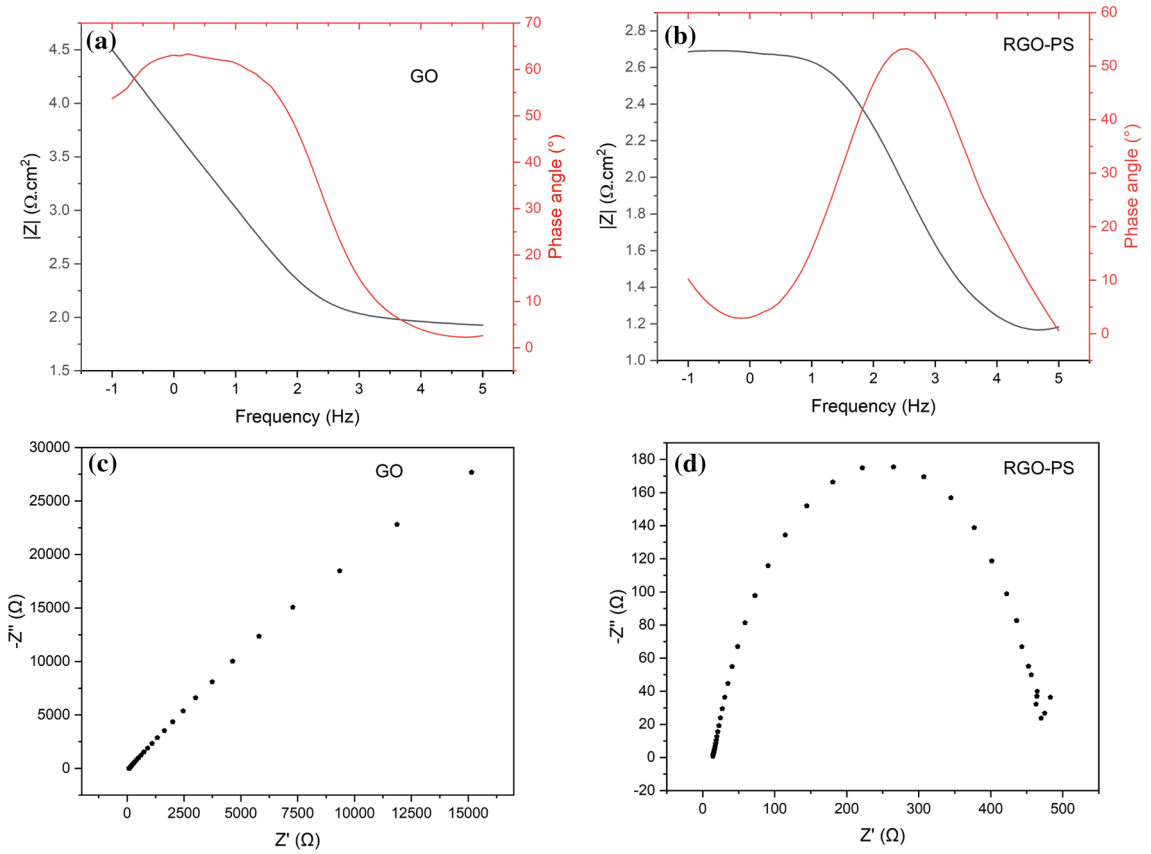

Fig. 14 Graph of Bode, phase and Nyquist plots for (a) GO and (b) RGO-PS.

or component, and the result will indicate how much resistance it provides to the flow of electrons (electric current). Bode and Nyquist graphical representations were used in this method for calculating the capacitance, consisting of the representation of log |*Z*| versus log ω, where Eq. 3 determines the impedance modulus |Z|.

$$|Z| = \sqrt{Zr^2 + Zi^2} \tag{3}$$

where *Zr* is real impedance and *Zi* is imaginary impedance.

It is well known that there is a change in the low-frequency peak for the GO sample to medium frequency for RGO-PS and that the phase angle decreases with the increase in frequency and approximation to 0° in the high-frequency region. However, the RGO-PS in the region of medium frequency reaches approximation of 50°, shown in Fig. 14a and b. This is typical behavior for a parallel circuit, as the impedance value in this region produces the electrolytic resistance (Re) between working and reference electrodes. Figure 14c and d compare the Nyquist plot of GO and RGO-PS electrodes. While the GO sample shows a slope line in the medium to high-frequency regions, the RGO-PS sample shows the formation of a semicircle in the medium frequency region, validating its charge storage mechanism dominated by faradaic redox reactions. This observation is in good agreement with its low-rate performance.[72] According to Casero et al.,[78] from these results, we concluded that the Bode and Nyquist diagrams constitute a method to determine whether graphene is in its unambiguously oxidized or reduced form.

The charge/discharge profile of the galvanostatic curves in the sweep rate between 10 eV and 200 eV and potential range from 0 V to 1 V is shown in Fig. 15a and b for GO and RGO-PS, respectively. Generally, the values of specific capacitance (Cs) found for RGO are in a range between 12 F g^{-1} and 27 F g^{-1}, according to the study by Gopalakrishnan et al. and Zhang et al.[79,80] However, Das et al.[81] found that the value of Cs was equal to 46 F g^{-1} when RGO was combined with MgO nanoparticles. GO, on the other hand, presents a capacitance close to 1 F g^{-1}.[81]

In this sense, using the specific capacitance equation which is obtained from the product of the discharge current integral with time variation by the mass product and power variation,[82] Cs values of 0.91 F g^{-1} were obtained for GO and 23.81 F g^{-1} for RGO-PS using the PS reducer. Therefore, in supercapacitor devices, RGO sheets show promise as a binder that improves ion adsorption capacity, as well as

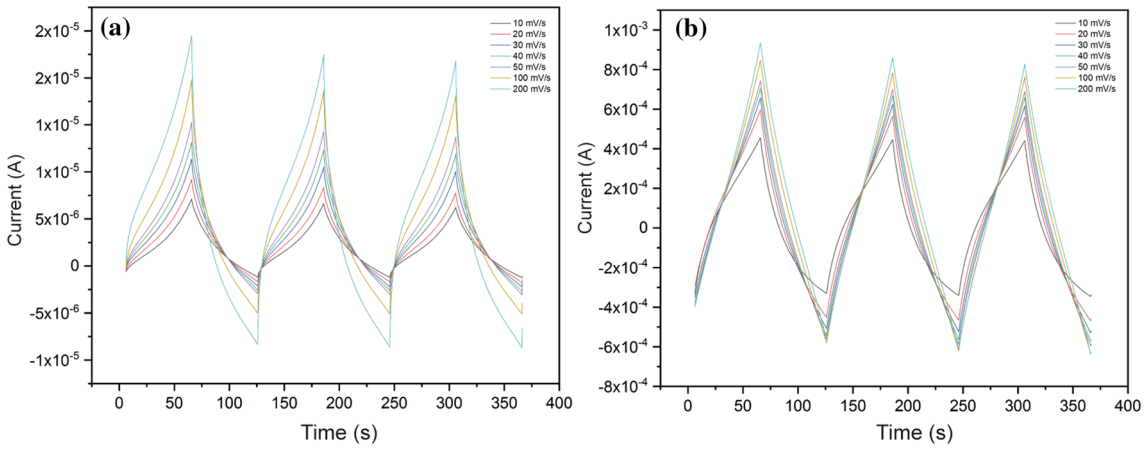

Fig. 15 Graph of charge/discharge profile of the galvanostatic curves for (a) GO and (b) RGO-PS.

in providing a route through which ions can easily pass to reach surfaces, leading to high capacitance and storage rates.

Conclusion

In this research, GO was synthesized by the modified method of Hummers and Hoffman. Based on the synthesis, the influence of new industrial reducing agents was evaluated in comparison with conventional reducers, seeking viable and efficient application in the reduction of GO. Microstructural, morphological and optical analyses were carried out, in addition to an electrochemical study. By XRD analysis, the interplanar distances showed the formation of GO and RGO, with the restoration of the ordered crystalline structure with formation of an intense peak in the region of $2\theta = 11.8°$ for GO and a displacement of the peak for $2\theta = 22.3°$ for RGO-PS. Raman spectroscopy for RGO-PS and RGO-SI showed the formation of a D band at 1580 cm^{-1} and a G band at 1351 cm^{-1}. FTIR spectroscopy showed the presence of carbonyl and hydroxyl bonds, confirming the formation of GO and the removal of oxide groups in the synthesis of RGO. HRTEM and FEG-SEM showed the presence of rough sheets of GO, and after reduction, they displayed similar fine characteristics which were randomly aggregated, with distinct edges, wrinkled surfaces and folding. The electrochemical analysis showed that the cyclic voltammetry of GO and the best RGO-PS reduction result at different scan rates revealed the formation of a rectangular geometry with an accentuated distance between the curves at higher scan rates. From this, the reducing agent derived from PS proved to be the most efficient and exhibited greater applicability, as it has superior microstructural, morphological, optical, electrochemical and thermal properties compared to the properties obtained from conventional reducing agents. Therefore, it can be proposed as a reducing agent using concepts of green and ecological processing in obtaining RGO with few sheets and excellent electrochemical properties.

Acknowledgments This study was supported by CnPQ—National Council for Scientific and Technological Development—45034/2020-3. The PPGEQ at the Federal University of Rio Grande do Norte.

Funding Not applicable.

Conflict of interest The authors declare that they have no conflict of interest.

Ethical Approval Not applicable.

References

1. D. Wei and J. Kivioja, Graphene for energy solutions and its industrialization. *Nanoscale* 5, 10108 (2013).
2. F. Schwierz, Graphene transistors. *Nat. Nanotechnol.* 5, 487 (2010).
3. G. Anagnostopoulos, J. Parthenios, K. Papagelis, and C. Galiotis, *Flexible Carbon-Based Electronics*. ed. P. Samorì, and V. Palermo (Weinheim: Wiley-VHC, 2018), p. 207.
4. Z. Yin, J. Zhu, Q. He, X. Cao, C. Tan, H. Chen, Q. Yan, and H. Zhang, Graphene-based materials for solar cell applications. *Adv. Energy Mater.* 4, 1300574 (2014).
5. M.F. El-Kady, Y. Shao, and R.B. Kaner, Graphene for batteries, supercapacitors and beyond. *Nat. Rev. Mater.* 1, 16033 (2016).
6. N. Izzaty, H. Y. Sastra, and Ilyas, in *IOP Conference Series: Materials Science and Engineering* (2019), p. 012133.
7. S. Kwon, Y.H. Hwang, M. Nam, H. Chae, H.S. Lee, Y. Jeon, S. Lee, C.Y. Kim, S. Choi, G. Jeong, and K.C. Choi, Recent progress of fiber shaped lighting devices for smart display applications—a fibertronic perspective. *Adv. Mater.* 32, 1903488 (2020).
8. W. Robertson, C.S. Allen, Y.A. Wu, K. He, J. Olivier, J. Neethling, A.I. Kirkland, and J.H. Warner, Spatial control of defect creation in graphene at the nanoscale. *Nat. Commun.* 3, 1144 (2012).
9. P. Avouris and C. Dimitrakopoulos, Graphene: synthesis and applications. *Mater. Today* 15, 86 (2012).
10. Y. Zhu, S. Murali, W. Cai, X. Li, J.W. Suk, J.R. Potts, and R.S. Ruoff, Graphene and graphene oxide: synthesis, properties, and applications. *Adv. Mater.* 22, 3906 (2010).

11. W.S. Hummers and R.E. Offeman, Preparation of graphitic oxide. *J. Am. Chem. Soc.* 6, 1339 (1958).
12. D.A. Dikin, S. Stankovich, E.J. Zimney, R.D. Piner, G.H.B. Dommett, G. Evmenenko, S.T. Nguyen, and R.S. Ruoff, Preparation and characterization of graphene oxide paper. *Nature* 448, 457 (2007).
13. B. Brodie, XIII. On the atomic weight of grafite. *Philos. Trans.* 149, 249 (1859).
14. L. Staudenmaier, Preparation of graphitic oxide. *Ber Dtsch Chem Ges* 31, 1481 (1898).
15. W. Gao, L.B. Alemany, L. Ci, and P.M. Ajayan, New insights into the structure and reduction of graphite oxide. *Nat. Chem.* 1, 403 (2009).
16. H. Yu, B. Zhang, C. Bulin, R. Li, and R. Xing, High-efficient synthesis of graphene oxide based on improved hummers method. *Sci. Rep.* 6, 1 (2016).
17. S. Sathyamoorthi, V. Suryanarayanan, and D. Velayutham, Electrochemical exfoliation and in situ carboxylic functionalization of graphite in non-fluoro ionic liquid for supercapacitor application. *J. Solid State Electrochem.* 18, 2789 (2014).
18. V. Sridhar, J.H. Jeon, and I.K. Oh, Synthesis of graphene nanosheets using eco-friendly chemicals and microwave radiation. *Carbon N Y* 48, 2953 (2010).
19. G. Wang, B. Wang, J. Park, J. Yang, X. Shen, and J. Yao, Synthesis of enhanced hydrophilic and hydrophobic graphene oxide nanosheets by a solvothermal method. *Carbon N Y* 47, 68 (2009).
20. D. Chen, H. Feng, and J. Li, Preparation, functionalization, and electrochemical applications. *Chem. Rev.* 112, 6027 (2012).
21. O.C. Compton and S.T. Nguyen, Graphene oxide, highly reduced graphene oxide, and graphene: versatile building blocks for carbon-based materials. *Small* 6, 711 (2010).
22. S. Pei and H.M. Cheng, The reduction of graphene oxide. *Carbon N Y* 50, 3210 (2012).
23. C.K. Chua and M. Pumera, Chemical reduction of graphene oxide: a synthetic chemistry viewpoint. *Chem. Soc. Rev.* 43, 291 (2014).
24. B.S. de Lima, M.I.B. Bernardi, and V.R. Mastelaro, Wavelength effect of ns-pulsed radiation on the reduction of graphene oxide. *Appl. Surf. Sci.* 506, 144808 (2020).
25. S. Park, Y. Hu, J.O. Hwang, E.S. Lee, L.B. Casabianca, W. Cai, J.R. Potts, H.W. Ha, S. Chen, J. Oh, S.O. Kim, Y.H. Kim, Y. Ishii, and R.S. Ruoff, Chemical structures of hydrazine-treated graphene oxide and generation of aromatic nitrogen doping. *Nat. Commun.* 3, 638 (2012).
26. H. Feng, R. Cheng, X. Zhao, X. Duan, and J. Li, A low-temperature method to produce highly reduced graphene oxide. *Nat. Commun.* 4, 1539 (2013).
27. H.J. Shin, K.K. Kim, A. Benayad, S.M. Yoon, H.K. Park, I.S. Jung, M.H. Jin, H.K. Jeong, J.M. Kim, J.Y. Choi, and Y.H. Lee, Efficient reduction of graphite oxide by sodium borohydride and its effect on electrical conductance. *Adv. Funct. Mater.* 19, 1987 (2009).
28. T. Zhou, F. Chen, K. Liu, H. Deng, Q. Zhang, J. Feng, and Q. Fu, A simple and efficient method to prepare graphene by reduction of graphite oxide with sodium hydrosulfite. *Nanotechnology* 22, 045704 (2010).
29. K.K.H. De Silva, H.H. Huang, and M. Yoshimura, Progress of reduction of graphene oxide by ascorbic acid. *Appl. Surf. Sci.* 447, 338 (2018).
30. D. Chen, L. Li, and L. Guo, An environment-friendly preparation of reduced graphene oxide nanosheets via amino acid. *Nanotechnology* 22, 325601 (2011).
31. O. Akhavan, E. Ghaderi, S. Aghayee, Y. Fereydooni, and A. Talebi, The use of a glucose-reduced graphene oxide suspension for photothermal cancer therapy. *J. Mater. Chem.* 22, 13773 (2012).
32. D. Suresh, Udayabhanu, M.A. Pavan Kumar, H. Nagabhushana, and S.C. Sharma, Cinnamon supported facile green reduction of graphene oxide, its dye elimination and antioxidant activities. *Mater. Lett.* 151, 93 (2015).
33. H.J. Chu, C.Y. Lee, and N.H. Tai, Green reduction of graphene oxide by *Hibiscus sabdariffa* L. to fabricate flexible graphene electrode. *Carbon N Y* 80, 725 (2014).
34. P. Chettri, V.S. Vendamani, A. Tripathi, A.P. Pathak, and A. Tiwari, Self assembly of functionalised graphene nanostructures by one step reduction of graphene oxide using aqueous extract of *Artemisia vulgaris*. *Appl. Surf. Sci.* 362, 221 (2016).
35. R.K. Upadhyay, N. Soin, G. Bhattacharya, S. Saha, A. Barman, and S.S. Roy, Grape extract assisted green synthesis of reduced graphene oxide for water treatment application. *Mater. Lett.* 160, 355 (2015).
36. D. Suresh, P.C. Nethravathi, A. Udayabhanu, H. Nagabhushana, and S.C. Sharma, Spinach assisted green reduction of graphene oxide and its antioxidant and dye absorption properties. *Ceram. Int.* 41, 4810 (2015).
37. V.S. Kindalkar, K.K.S. Bhat, and S.M. Dharmaprakash, An eco-friendly approach for the reduction of graphene oxide using *Syzygium samarangense* fruit extract. *Mater. Chem. Phys.* 261, 124224 (2021).
38. P. Parthipan, L. Cheng, A. Rajasekar, M. Govarthanan, and A. Subramania, Biologically reduced graphene oxide as a green and easily available photocatalyst for degradation of organic dyes. *Environ. Res.* 196, 110983 (2021).
39. S. Abdolhosseinzadeh, H. Asgharzadeh, and H.S. Kim, Fast and fully-scalable synthesis of reduced graphene oxide. *Sci. Rep.* 5, 10160 (2015).
40. T. Zhou, F. Chen, C. Tang, H. Bai, Q. Zhang, H. Deng, and Q. Fu, The preparation of high performance and conductive poly (vinyl alcohol)/graphene nanocomposite via reducing graphite oxide with sodium hydrosulfite. *Compos. Sci. Technol.* 71, 1266 (2011).
41. M. Strankowski, D. Włodarczyk, Ł Piszczyk, and J. Strankowska, Polyurethane nanocomposites containing reduced graphene oxide, FTIR, Raman, and XRD studies. *J. Spectrosc.* 2016, 1 (2016).
42. B.S. Mohan, K. Ravi, R.B. Anjaneyulu, G.S. Sree, and K. Basavaiah, Fe_2O_3/RGO nanocomposite photocatalyst: effective degradation of 4-Nitrophenol. *Physica B Condens. Matter.* 553, 190 (2019).
43. J. Chen, B. Yao, C. Li, and G. Shi, An improved Hummers method for eco-friendly synthesis of graphene oxide. *Carbon N Y* 64, 225 (2013).
44. K.P. Aryal and H.K. Jeong, Simultaneous determination of ascorbic acid, dopamine, and uric acid with polyaniline/hemin/reduced graphite oxide composite. *Chem. Phys. Lett.* 768, 138405 (2021).
45. R. Al-Gaashani, A. Najjar, Y. Zakaria, S. Mansour, and M.A. Atieh, XPS and structural studies of high quality graphene oxide and reduced graphene oxide prepared by different chemical oxidation methods. *Ceram. Int.* 45, 14439 (2019).
46. L. Sun, H. Yu, and B. Fugetsu, Graphene oxide adsorption enhanced by in situ reduction with sodium hydrosulfite to remove acridine orange from aqueous solution. *J. Hazard. Mater.* 203–204, 101 (2012).
47. N. Díez, A. Śliwak, S. Gryglewicz, B. Grzyb, and G. Gryglewicz, Enhanced reduction of graphene oxide by high-pressure hydrothermal treatment. *RSC Adv.* 5, 81831 (2015).
48. Siklitskaya, E. Gacka, D. Larowska, M. Mazurkiewicz-Pawlicka, A. Malolepszy, L. Stobiński, B. Marciniak, A. Lewandowska-Andrałojć, A. Kubas, L. Stobiński et al., Lerf–Klinowski-type models of graphene oxide and reduced graphene oxide are robust in analyzing non-covalent functionalization with porphyrins. *Sci. Rep.* 11, 7977 (2021).
49. S. Drewniak, R. Muzyka, A. Stolarczyk, T. Pustelny, M. Kotyczka-Morańska, and M. Setkiewicz, Studies of reduced graphene oxide

and graphite oxide in the aspect of their possible application in gas sensors. *Sensors (Switzerland)* 16, 103 (2016).
50. M.K. Rabchinskii, A.T. Dideikin, D.A. Kirilenko, M.V. Baidakova, V.V. Shnitov, F. Roth, S.V. Konyakhin, N.A. Besedina, S.I. Pavlov, R.A. Kuricyn, N.M. Lebedeva, P.N. Brunkov, and A.Y. Vul, Facile reduction of graphene oxide suspensions and films using glass wafers. *Sci. Rep.* 8, 14154 (2018).
51. C. Xu, X. Shi, A. Ji, L. Shi, C. Zhou, and Y. Cui, Fabrication and characteristics of reduced graphene oxide produced with different green reductants. *PLoS ONE* 10, e0144842 (2015).
52. K.S. Kim, Y. Zhao, H. Jang, S.Y. Lee, J.M. Kim, K.S. Kim, J.H. Ahn, P. Kim, J.Y. Choi, and B.H. Hong, Large-scale pattern growth of graphene films for stretchable transparent electrodes. *Nature* 457, 706 (2009).
53. E. Salih, M. Mekawy, R.Y.A. Hassan, and I.M. El-Sherbiny, Synthesis, characterization and electrochemical-sensor applications of zinc oxide/graphene oxide nanocomposite. *J. Nanostruct. Chem.* 6, 137 (2016).
54. S. Saxena, T.A. Tyson, S. Shukla, E. Negusse, H. Chen, and J. Bai, Investigation of structural and electronic properties of graphene oxide. *Appl. Phys. Lett.* 99, 1 (2011).
55. N.R. Wilson, P.A. Pandey, R. Beanland, R.J. Young, I.A. Kinloch, L. Gong, Z. Liu, K. Suenaga, J.P. Rourke, S.J. York, and J. Sloan, Graphene oxide: structural analysis and application as a highly transparent support for electron microscopy. *ACS Nano* 3, 2547 (2009).
56. Shalaby, D. Nihtianova, P. Markov, A.D. Staneva, R.S. Iordanova, and Y.B. Dimitriev, Structural analysis of reduced graphene oxide by transmission electron microscopy. *Bulg. Chem. Commun.* 47, 291 (2015).
57. C. Chen, Y.C. Chen, Y.T. Hong, T.W. Lee, and J.F. Huang, Facile fabrication of ascorbic acid reduced graphene oxide-modified electrodes toward electroanalytical determination of sulfamethoxazole in aqueous environments. *Chem. Eng. J.* 352, 188 (2018).
58. V.B. Mohan, K. Jayaraman, and D. Bhattacharyya, Brunauer–Emmett–Teller (BET) specific surface area analysis of different graphene materials: a comparison to their structural regularity and electrical properties. *Solid State Commun.* 320, 114004 (2020).
59. J. Zhao, Y. Zhu, F. Pan, G. He, C. Fang, K. Cao, R. Xing, and Z. Jiang, Fabricating graphene oxide-based ultrathin hybrid membrane for pervaporation dehydration via layer-by-layer self-assembly driven by multiple interactions. *J. Membr. Sci.* 487, 162 (2015).
60. M.P. More and P.K. Deshmukh, Quality by design approach for the synthesis of graphene oxide nanosheets using full factorial design with enhanced delivery of Gefitinib nanocrystals. *Mater. Res. Express* 8, 075602 (2021).
61. R. Hack, C.H.G. Correia, R.A.D.S. Zanon, and S.H. Pezzin, Characterization of graphene nanosheets obtained by a modified Hummer's method. *Rev. Mater.* 23, e11988 (2018).
62. B.S. Lee, Y. Lee, J.Y. Hwang, and Y.C. Choi, Structural properties of reduced graphene oxides prepared using various reducing agents. *Carbon Lett.* 16, 255 (2015).
63. Z. Ismail, Green reduction of graphene oxide by plant extracts: a short review. *Ceram. Int.* 45, 23857 (2019).
64. F. Baskoro, C.B. Wong, S.R. Kumar, C.W. Chang, C.H. Chen, D.W. Chen, and S.J. Lue, Graphene oxide–cation interaction: inter-layer spacing and zeta potential changes in response to various salt solutions. *J. Memb. Sci.* 554, 253 (2018).
65. S. Ahmad, A. Ahmad, S. Khan, S. Ahmad, I. Khan, S. Zada, and P. Fu, Algal extracts based biogenic synthesis of reduced graphene oxides (rGO) with enhanced heavy metals adsorption capability. *J. Ind. Eng. Chem.* 72, 117 (2019).
66. L. Cao, Z. Li, K. Su, and B. Cheng, Hydrophilic graphene preparation from gallic acid modified graphene oxide in magnesium self-propagating high temperature synthesis process. *Sci. Rep.* 6, 35184 (2016).
67. N. M. S. Hidayah, W. W. Liu, C. W. Lai, N. Z. Noriman, C. S. Khe, U. Hashim, and H. C. Lee, in *AIP Conference Proceedings* (2017), p. 020033.
68. H. Saleem, M. Haneef, and H.Y. Abbasi, Synthesis route of reduced graphene oxide via thermal reduction of chemically exfoliated graphene oxide. *Mater. Chem. Phys.* 204, 1 (2018).
69. V. Gupta, N. Sharma, U. Singh, M. Arif, and A. Singh, Higher oxidation level in graphene oxide. *Optik (Stuttg)* 143, 115 (2017).
70. M.E. Assal, M.R. Shaik, M. Kuniyil, M. Khan, A. Al-Warthan, M.R.H. Siddiqui, S.M.A. Khan, W. Tremel, M.N. Tahir, and S.F. Adil, A highly reduced graphene oxide/ZrO_x–$MnCO_3$ or -Mn_2O_3 nanocomposite as an efficient catalyst for selective aerial oxidation of benzylic alcohols. *RSC Adv.* 7, 55336 (2017).
71. Kaniyoor, T.T. Baby, T. Arockiadoss, N. Rajalakshmi, and S. Ramaprabhu, Graphenes: a study on the effects of synthesis parameters on exfoliation–reduction of graphite oxide. *J. Phys. Chem. C* 115, 17660 (2011).
72. Hussein, S. Sarkar, D. Oh, K. Lee, and B. Kim, Epoxy/p-phenylenediamine functionalized graphene oxide composites and evaluation of their fracture toughness and tensile properties. *J. Appl. Polym. Sci.* 133, 1 (2016).
73. Z. Lei, L. Lu, and X.S. Zhao, The electrocapacitive properties of graphene oxide reduced by urea. *Energy Environ. Sci.* 5, 6391 (2012).
74. J.H. Choi, C. Lee, S. Cho, G.D. Moon, B. Sukim, H. Chang, and H.D. Jang, High capacitance and energy density supercapacitor based on biomass-derived activated carbons with reduced graphene oxide binder. *Carbon N Y* 132, 16 (2018).
75. X. Zhu, J. Xu, X. Duan, L. Lu, K. Zhang, Y. Yu, H. Xing, Y. Gao, L. Dong, H. Sun, and T. Yang, Controlled synthesis of partially reduced graphene oxide: enhance electrochemical determination of isoniazid with high sensitivity and stability. *J. Electroanal. Chem.* 757, 183 (2015).
76. B. Xu, S. Yue, Z. Sui, X. Zhang, S. Hou, G. Cao, and Y. Yang, What is the choice for supercapacitors: Graphene or graphene oxide? *Energy Environ. Sci.* 4, 2826 (2011).
77. C. Couly, M. Alhabeb, K.L. Van Aken, N. Kurra, L. Gomes, A.M. Navarro-Suárez, B. Anasori, H.N. Alshareef, and Y. Gogotsi, Asymmetric flexible MXene-reduced graphene oxide micro-supercapacitor. *Adv. Electron. Mater.* 4, 480 (2018).
78. E. Casero, A.M. Parra-Alfambra, M.D. Petit-Domínguez, F. Pariente, E. Lorenzo, and C. Alonso, Differentiation between graphene oxide and reduced graphene by electrochemical impedance spectroscopy (EIS). *Electrochem. Commun.* 20, 63 (2012).
79. Gopalakrishnan, P. Sahatiya, and S. Badhulika, Low temperature, one-pot green synthesis of tailored carbon nanostructures/reduced graphene oxide composites and its investigation for supercapacitor application. *Mater. Lett.* 198, 46 (2017).
80. W. Zhang, Y. Zhang, Y. Tian, Z. Yang, Q. Xiao, X. Guo, L. Jing, Y. Zhao, Y. Yan, J. Feng, and K. Sun, Insight into the capacitive properties of reduced graphene oxide. *ACS Appl. Mater. Interfaces* 6, 2248 (2014).
81. P.S. Das, S. Bakuli, I. Biswas, A.K. Mallik, A. Dey, S. Mukherjee, J. Ghosh, and A.K. Mukhopadhyay, RGO/MgO hybrid nanocomposites with high specific capacitance. *Ceram. Int.* 44, 424 (2018).
82. L. Buglione, E.L.K. Chng, A. Ambrosi, Z. Sofer, and M. Pumera, Graphene materials preparation methods have dramatic influence upon their capacitance. *Electrochem. Commun.* 14, 5 (2012).